AIChE WILEY InterScience DISCOVER SOMETHING GREAT

Temporally-Resolved Inkjet Drop Impaction on Surfaces

Hongming Dong, Wallace W. Carr, and David G. Bucknall
School of Polymer, Textile and Fiber Engineering, Georgia Institute of Technology, Atlanta, GA 30332

Jeffrey F. Morris
Benjamin Levich Institute and Dept. of Chemical Engineering, City College of CUNY, New York, NY 10031

DOI 10.1002/aic.11283
Published online August 29, 2007 in Wiley InterScience (www.interscience.wiley.com).

Impaction on smooth solid substrates of drops formed by the drop-on-demand (DOD) method was investigated over a wide range of impaction speeds (U_0 = 2.21–12.2 m/s), surface contact angles (θ = 6–107°), and drop diameters (D_0 = 40.8–50.5 μm). The experimental results were compared with several existing equations for predicting maximum spreading. The dimensionless time to reach maximum spreading ratio, scaled by D_0/U_0, ranged from 0.6 to 2.99, depending on Weber number and contact angle. Micron and millimeter drop impactions were compared, and the results indicate that scaling based on three dimensionless numbers (We, Re or Oh, and cos θ) is valid, but spreading ratios of millimeter drops are usually slightly larger during the whole process. The difference is ascribed mainly to the effect of gravity. © 2007 American Institute of Chemical Engineers *AIChE J*, 53: 2606–2617, 2007
Keywords: drop impaction, inkjet printing, micron drop

Introduction

Drop impaction on surfaces has received extensive attention for over one century since Worthington observed and recorded the patterns left by water, milk, and mercury drop impaction on smoked and unsmoked glass plates.[1,2] For perpendicular impact as considered here, various behaviors are observed depending on the circumstances of impaction.[3,4] In most cases, the drop spreads, retracts and oscillates to the equilibrium state. Other possible outcomes of drop impaction are rebounding, bouncing and splashing. The outcomes of the collision are determined by many factors, including the properties of the liquid, size and speed of the drop, properties of the substrate, such as relative smoothness or roughness, and liquid/substrate interactions, which are characterized by static and/or dynamic contact angle(s). The significant drop parameters thus include viscosity, surface tension, impact speed, drop size, temperature, and additives, such as surfactants and polymers.[5] The parameters related to the substrate consist of roughness (including topography and porosity), surface chemistry, and temperature.

Dimensional analysis[6] shows that the impaction process of Newtonian fluids is governed primarily by conditions, which may be described by three independent dimensionless numbers, specifically the Weber number (We), Reynolds number (Re) or Ohnesorge number (Oh), and dynamic contact angle (ψ, which is equal to the static contact angle, denoted θ, at equilibrium). These dimensionless numbers are defined as follows

$$We = \frac{\rho U_0^2 D_0}{\gamma}; \quad Oh = \frac{\mu}{\sqrt{\rho \gamma D_0}} \text{ or}$$
$$Re = \sqrt{We}/Oh = \frac{\rho U_0 D_0}{\mu}; \cos\theta = \frac{\gamma_{SV} - \gamma_{SL}}{\gamma}$$

where U_0 is drop impaction speed, D_0 is diameter of the spherical drop prior to impact, μ is liquid viscosity, γ is surface tension (or surface energy per unit area) of the drop liquid, ρ is liquid density, γ_{SV} is interfacial energy between the substrate and air, and γ_{SL} is interfacial energy between

Correspondence concerning this article should be addressed to W. Carr at chuck.carr@ptfe.gatech.edu.

the substrate and liquid. Note that drop radius instead of drop diameter is used as the characteristic length in *Re* and *We* by some investigators, e.g. Schiaffino and Sonin.[6]

Most of the previous experimental studies of drop impaction on surfaces were conducted in the millimeter-scale regime. In inkjet printing and other applications, however, drop size ranges from several microns to several hundred microns. Therefore, the investigation of drop impactions at the application scale, i.e. the micron-scale, is needed to determine the applicability of rich millimeter drop results to micron drop impaction.

Several equations[7–14] are available to estimate the maximum spreading ratio, $D^*_{max} = D_{max}/D_0$, where D_{max} is the maximum diameter of the contact area of the drop on the substrate. Predictions of seven of these equations[7–13] (see Table 1) will be compared with our experimental results. The equation of Scheller and Bousfield[8] was obtained by correlating their experimental results against the dimensionless group Re^2Oh. The role of contact angle was ignored. The equation of Chandra and Avedisian[7] was based on an energy conservation equation, and the assumptions that drop volume is conserved and the drop spreads into a cylindrical disk. Viscous dissipation energy was approximated using a dissipation function and several assumptions. To improve agreement with their experimental results, Pasandideh-Fard et al.[9] modified the equation of Chandra and Avedisian[7] by changing the viscous dissipation energy term. They assumed that liquid motion in the droplet can be represented by axisymmetric stagnation-point flow. Mao et al.[10] modified the equation of Pasandideh-Fard et al. by using an empirical expression to evaluate viscous dissipation energy. Coefficients in the empirical expression were adjusted to best fit their data. Fukai et al.[11] used an expression having the analytical form of the model of Chandra and Avedisian, and determined three coefficients to best fit their numerical data. Park et al.[13] derived equations based on the work of Mao et al.[10] However, the shape of the drop was assumed to be a spherical cap and a term accounting for interfacial energy change during spontaneous spreading was added to the energy balance. When compared to predictions of equations in the literature, the relationships of Park et al.[13] gave better predictions for low-drop impact velocity. Roisman et al.[12] modeled the drop impaction process to predict the evolution of the drop diameter. Mass and momentum equations were used, taking into account the effects of initial, viscous and surface forces, and wettability. A simplified approximation for the maximum spreading ratio was obtained. In this paper, our micron-drop impaction experimental results will be compared with these equations.

There have been several notable studies[14–17] directed toward the smaller scale drops. Asai et al.[14] examined spreading of micron size drops from a piezoelectric inkjet printhead impacting on moving paper, and obtained a simple correlation formula to predict the maximum spreading ratio.

These studies provide useful, but still relatively limited, information about the micron-scale drop impaction process. Further understanding of the dynamics of micron drop impaction on surfaces is important in the control of drop deposition on substrates; note that in going from a one-millimeter to a 50-μm dia. drop typical of inkjet methods, the volume is reduced by a factor of 8,000, suggesting the capability to apply very precisely small amounts of materials by the drop-on-demand (DOD) technology. Here, we consider only the simplest case of Newtonian liquid drop impact, but the interest in this capability and desire to apply it to a range of materials, including dispersions and complex fluids, motivates our study of the process at the application scale. The objectives of this work are to examine the characteristics of the micron-scale drop impaction process, based on a series of comprehensive experiments and demonstrate the ability to resolve the dynamics of these small drops, as well as determine the scalability of the impaction process from millimeter to micron drops. In general, we expect that scaling analysis will hold, and gross features of the phenomena will be the same. However, the surface-to-volume ratio, scaling inversely with the drop diameter, is so much larger for the smaller drops that issues associated with either the surfaces themselves, or with the balance of surface-to-volume forces may require care in their consideration. By considering both cases here, we are able to assess certain of these issues. The smallness of the drops, while creating difficulty experimentally, has the expected simplifying feature of justifying neglect of gravity in their analysis. More significantly, the potential for phenomena associated with the surfaces which are obscured at the larger scale, whether due to air-liquid and solid-liquid surface energies, interaction with small-scale solid surface morphology, or issues we have not considered, makes probing at this scale with the Newtonian fluid of interest. Future work will address more complex mixtures.

A high-speed photography imaging system coupled with a motorized stage was used,[18,19] which allows visualization of the micron drop impaction process with a temporal resolution as low as 200 ns and spatial resolution of 0.81 μm/pixel. The whole system provides significantly better resolution and reproducibility than those utilized in previous studies. In addition, in this study, surfaces with a wide range of contact angles (both hydrophilic and hydrophobic) are used. The corresponding dimensionless parameters lie in the ranges: $O(10) < Re < O(10^3)$ and $O(1) < \mathrm{We} < O(10^2)$. The experimental results are compared with predictions of several existing models and conclusions of prior work obtained using millimeter scale drops to examine their applicability for micron-scale drop impaction. Finally, micron drop impaction is compared against our own experiments with drops of millimeter size to examine the validity of description of the process using the dimensionless parameters of Reynolds and Weber number with equilibrium contact angle.

Experimental

Apparatus

Drops were generated using a piezoelectric actuated inkjet printhead. The nozzle exit diameter is about 53 μm. The method used for visualizing micron drop impaction was based on flash photography. A detailed introduction and analysis of the entire experimental setup is given in Dong et al.[20]; the temporal and spatial resolution are 200 ns and 0.81 μm/pixel.

Millimeter-scale drops which were generated using a dripping method were also studied. The liquid was pushed out of a syringe with a 28-gauge needle (inner and outer diameters of 0.18 and 0.36 mm) at a flow rate of 0.02 ml/min, producing a drop with a diameter of about 2.23 mm. Drop impact

Table 1. Equations of Maximum Spreading Ratio

Reference	Equation	Type	Drop Size	Approach/Assumptions	Contact Angle
Chandra & Avedisian (1991)	$\frac{3}{2}\frac{We}{Re}D^{*}_{mans}{}^{4}+(1-\cos\theta)D^{*}_{\max}{}^{2}-\left(\frac{We}{3}+4\right)=0$	Analytical	~1.5 mm	Energy conservation, Drop has a cylindrical profile at maximum spreading position, Viscous dissipation based on the linear velocity profile	Static contact angle
Asai et al. (1993)	$D^{*}_{\max}=1+0.48We^{0.5}\exp[-1.48We^{0.22}\,Re^{-.021}]$	Empirical	44–81 μm	—	Not included
Scheller & Bousfield (1995)	$D^{*}_{\max}=0.61(Re^{2}\,Oh)^{0.166}$	Empirical	2.0–4.0 mm	—	Not included
Pasandideh-Fard et al. (1996)	$D^{*}_{\max}=\left[\frac{We+12}{3(1-\cos\theta_a)+4We/\sqrt{Re}}\right]^{1/2}$	Analytical	~ 2.0 mm	Same as Chandra & Avedisian (1991), except that viscous dissipation is based on the velocity profile of stagnation-point flow	Advancing contact angle
Mao et al. (1997)	$\left[\frac{1}{4}(1-\cos\theta)+0.2\frac{We^{0.83}}{Re^{0.33}}\right]D^{*}_{\max}3-\left(\frac{We}{12}+1\right)D^{*}_{\max}+\frac{2}{3}=0$	Semi-empirical	1.5–3.5 mm	Same as Pasandideh-Fard et al. (1996), except using an empirical expression to evaluate viscous dissipation energy	Static contact angle
Fukai et al. (1998)	$\frac{1}{2}\frac{We}{Re^{0.772}}D^{*}_{mans}{}^{4}+2.29(1-\cos\theta)D^{*}_{\max}{}^{2}-\left(\frac{We}{3}+4\right)=0$	Semi-empirical	Not given	Same as Chandra & Avedisian (1991), except that three empirical coefficients were determined for experiments	Static contact angle
Roisman et al. (2002)	$D^{*}_{\max}=\frac{\overline{D}_1}{2}+\frac{\sqrt{6}A\overline{D}_1{}^{2}}{4}\sqrt{\frac{1-\cos\langle\theta\rangle}{We}}+\frac{\sqrt{6}}{24A}\sqrt{\frac{We}{1-\cos\langle\theta\rangle}}$ Where $\langle\theta\rangle$ is the dynamic contact angle, $\overline{D}_1$ and A is determined from We, Re and $\langle\theta\rangle$	Analytical	1.96–3.17 mm	Momentum and energy conservation, Spreading drop has cylindrical profile, Viscous creeping flow between tow approaching discs; Work performed by the radial forces applied from the wall to the contact line is included	Dynamics contact angle, calculated using Hoffman's law
Park et al. (2003)	$\left[0.33\frac{We}{\sqrt{Re}}-\frac{1}{4}\cos\theta+\frac{1}{2}\left(\frac{1-\cos\alpha}{\sin^2\alpha}\right)\right]D^{*}_{\max}{}^{2}-1-\frac{We}{12}+\frac{\Delta E_{diss}}{\pi d^2\gamma}=0$ for $Re\geq 9D^{*}_{\max}{}^{4}$	Analytical	~2.3 mm	Same as Mao et al. (1997), except that 1) drop shape is a spherical cap, and 2) energy decrease during spontaneous spreading is added	Static contact angle

Table 2. Experimental Parameters for Micron and Millimeter Drop Impaction

Micron Drop						Millimeter Drop					
Liquid[a]	Impact Speed (m/s)	Drop Size (um)	*Re*	*We*	*Oh*	Liquids[b]	Viscosity (mPa·s)	Impaction Speed (m/s)	Drop Size (mm)	*Re*	*We*	*Oh*
Distilled water	2.21	40.9	100.9	2.77	0.0165	Mixture 1 (Glycerin/water 53/47)	6.7	0.27	2.23	101.6	2.74	0.0163
	4.36	48.8	238	12.8	0.0151	Mixture 2 (Glycerin/water 50/50)	6.1	0.58	2.23	241	12.7	0.0148
	12.2	50.5	689	103	0.0148	Mixture 3 (Glycerin/water 49.5/50.5)	6.0	1.67	2.23	700	105	0.0146

[a]For distilled water, density = 1.0 g/cm^3, viscosity = 0.893 mPa·s, surface tension = 72 mN/m at a temperature of 25°C.
[b]For three mixtures, density = 1.13 g/cm^3, surface tension = 67 mN/m.[27]

speed was changed by varying the distance of the nozzle tip from the impacted substrate. A CCD camera (Photron, 1280 × 1024 pixels) was used to continuously record the whole impaction process at the speed of 4,000 fps and exposure time of 1/32,000 s. The spatial resolution of the imaging system was 26.6 μm/pixel.

Materials

Micron drop impaction experiments were conducted using distilled water with three different drop sizes, each having a different impact speed (see Table 2). The different velocities and diameters were obtained by varying the signal amplitude sent to the piezoelectric transducer.[19] The corresponding ranges of Reynolds number *Re*, and Weber number *We*, were 10–1,000 and 1–100, respectively, which cover a typical regime for inkjet printing.[11] At a drop speed of 2.21 m/s, a single drop is generated for each driving pulse. Since no satellite is generated, the impaction process can be observed for times from contact up to approximately 13,000 μs. For longer times, the errors in the delay times produced by the delay generator are larger than camera exposure time (1 μs in most cases), and the camera and laser are no longer synchronized. The observation time is sufficient to record the effects of impaction, but the drops on the low contact angle surfaces have not reached their equilibrium positions at the end of the observation period. At drop speeds of 4.36 and 12.2 m/s, satellites are produced; thus, observation times from primary drop impaction until the first satellite reaches the substrates are limited to 800 μs and 120 μs, respectively. Despite these short time windows, they are sufficient to observe the main stages of the micron-scale drop impaction. The drops are produced in a sequence at fixed frequency and impact on fresh surface through motion of the substrate by a motorized stage. Due to the slow response of the motorized stage to an external triggering signal and the requirements of reproducibility, for each delay time setting, the frequency of drop generation was set at 2 Hz. A 20-signal train with a frequency of 2 Hz was applied to trigger the imaging system and motorized stage. The last ten images were used to obtain the experimental data, thereby avoiding the "first drop problem" as described in Dong et al.[20]

In order to identify the distinct characteristics of micron-scale drop impaction, millimeter- and micron-scale impaction studies were conducted at the same values of *Oh* (or *Re*) and *We*. The millimeter drop experiments were conducted using the drop with a dia. 2.23 mm, and liquid properties and drop speed were adjusted to obtain the desired values of *Re* and *We*. Mixtures of glycerin and water were selected as the working liquids. The experimental parameters for the millimeter drop impaction tests are listed in Table 2.

Five solid surfaces including glass slides (Fisher), thermal oxidized silicon wafer, and three self-assembled monolayers (SAMs) on gold coated silicon wafers were used as substrates for drop impaction. The contact angles of water and water/glycerin on these surfaces for the various concentrations used are listed in Table 3. The roughness (R) of five substrates was measured using atomic force microscope (AFM, Pacific Nanotechnology), and the results are presented in Table 3. Since $R/D_0 \sim O(10^{-5})$, the effect of roughness on the impaction process is negligible. Silicon wafers were treated to produce a layer of thermal oxide on the silicon wafer, which makes the surface more stable; oxidation of the surface of the silicon wafer was performed for four hours in a thermal oxidation furnace containing dry O_2 at a temperature of about 1,000°C. The monolayers were prepared by immersing freshly evaporated gold-coated (about 1,000 Å depth) silicon wafers into 1 mM solution of thiols in ethanol for 12 h.[21] Before the thermal evaporation of gold, the silicon wafer was precoated with chromium (about 50 Å in thickness) to improve the adhesion. The samples were washed with ethanol and blown dry with a stream of N_2. The two thiols, 11-mercapto-1-undecanol [$HS(CH_2)_{11}OH$] and 1-octadecanethiol [$CH_3(CH_2)_{17}SH$], were used to vary the amounts of hydrophilic ($-OH$) and hydrophobic ($-CH_3$) groups in the monolayer.[22] The contact angle of water on the monolayers varied with the content of the two thiols in solution, as shown in Table 3.

Table 3. Equilibrium Contact Angles of Water and Mixture of Water and Glycerin on Surfaces

Impacted Substrates	Contact Angle of Water (°)	Contact Angle of Glycerin/ Water Mixtures (°)	Roughness (nm)
Glass slide	~6	–	0.5
Thermally oxidized silicon wafer	31 ± 2	24 ± 2	0.8
9:1 OH/CH_3 SAM on gold coated silicon wafer	67 ± 2	62 ± 2	2.3
7:1 OH/CH_3 SAM on gold coated silicon wafer	88 ± 2	–	2.1
100% CH_3 SAM on gold coated silicon wafer	107 ± 2	99 ± 2	3.0

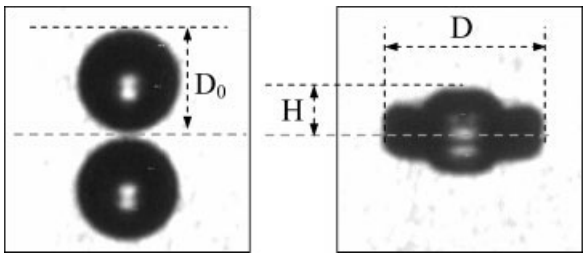

Figure 1. Drop shape before and after impact.

Surfaces with small contact angles, such as thermally oxidized silicon wafers and glass slides, are easily contaminated due to the adsorption of gas and dust. Thus, their contact angles increase gradually with storage time, for example, in one case the contact angle for thermal oxide coated silicon wafer was observed to increase from 31 to 70°. The following procedures were conducted to clean surfaces with low contact angles: The surfaces were soaked in NanoStrip (Cyantek Corp.) at 60°C for 30 min, then rinsed extensively with distilled water, and finally blown dry with N_2. The freshly-cleaned surfaces had constant contact angles for approximately 4 h. The impaction tests were conducted during this period. After that, the surface was cleaned again. Other surfaces (with a contact angle larger than 60°) could be re-used if they were cleaned with ethanol and blown dry with N_2 just before use; however, the contact angle was measured before every test to ensure that the surface had not been contaminated (and contact angle changed).

Imaging process and data analysis

The reported experimental results are based on images captured by the high-speed imaging system. The diameter of the contact area and the height of the drop above the substrate after impaction (see Figure 1) were measured to obtain the impaction curves as many other workers have done. In order to convert pixel values to positional values in X-Y coordinates, the image system was calibrated using a standard micron ruler (1-mm Nikon Stage Micrometer) to determine the distance per pixel in the focus plane.

Results and Discussion

Entire process of micron-scale drop impaction

Sequential images of water drop impaction for three different impact speeds (2.21, 4.36, and 12.2 m/s), corresponding to $1 < We < 100$ and $100 < Re < 1{,}000$, on five surfaces (contact angles of 6°, 31°, 67°, 88°, and 107°) are shown in Figure 2. The variation of dimensionless diameter or spread-

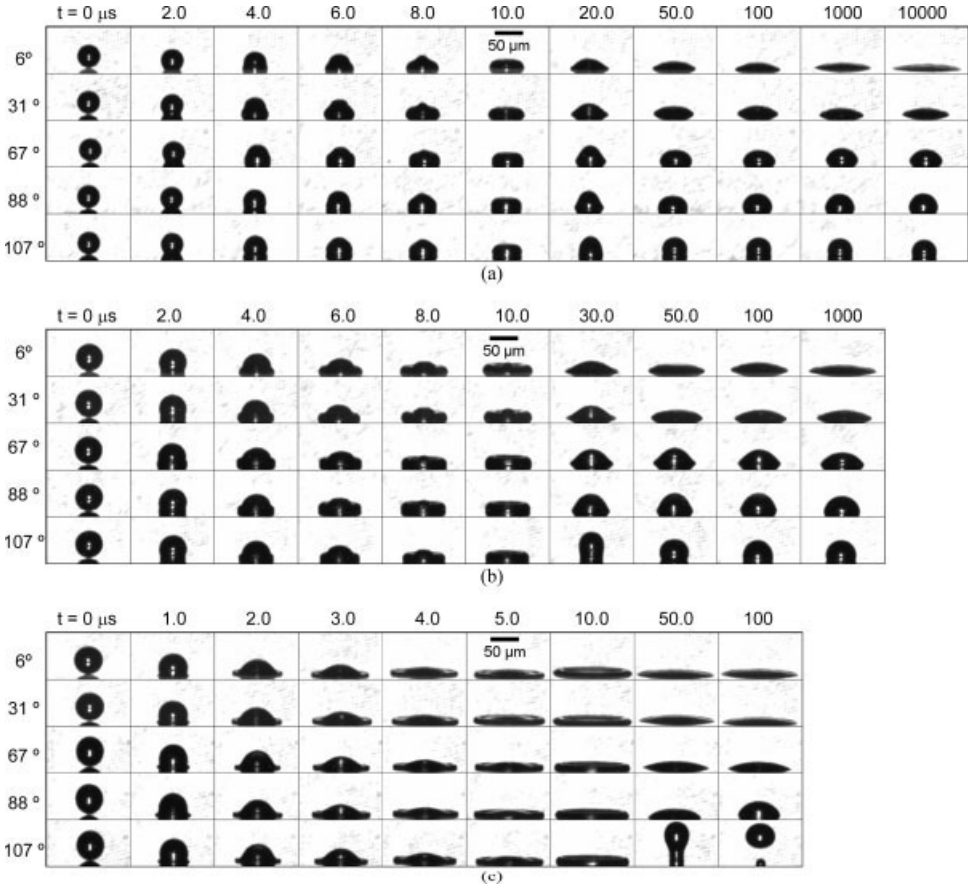

Figure 2. Sequence of images for drop impaction on five substrates: (a) U_0 = 2.21 m/s, D_0 = 40.9 μm; (b) U_0 = 4.36 m/s, D_0 = 48.8 μm; (c) U_0 = 12.2 m/s, D_0 = 50.5 μm.

Note that the scale bars are not identical. The observation angle of camera was set at about 10° from the horizontal substrate.

ing ratio ($D^* = D/D_0$) and dimensionless height ($H^* = H/D_0$) with time are plotted in Figure 3. Although the same DOD drop generator is used in each case, drop size varies from 40.9 to 50.5 μm under different driving voltage amplitudes required to produce the three drop speeds.

When a micron-scale drop contacts the substrate, the contact area of the drop rapidly moves outward, with a drop cross-section initially resembling a truncated sphere. As the liquid continues to move radially outward, a nearly flat layer is formed with a shape dependent on both impact speed and surface characteristics. For higher impact speeds and/or lower contact angle surfaces, the layer spreads faster and further and, is, therefore, thinner at maximum spreading. The layer remains at maximum spreading for a short time, causing a flattening in the impaction curves (see Figure 3). The entire spreading stage lasts $O(10)$ μs, and then the drop retracts under the action of surface tension. The height of the liquid layer increases gradually, and the contact area of the layer on the substrate contracts. The extent of retraction depends on the impact speed, as well as the wettability of the substrate, indicated by the contact angle. On the hydrophobic surface with a contact angle of 107°, the extent of retraction increases with impact speed. Under an impact speed of 12.2 m/s, the drop recedes strongly and most of the drop separates from the substrate, a phenomenon which is referred to as rebounding. Retraction weakens as the contact angle decreases, especially at an impact speed of 12.2 m/s. After impaction on the low-contact angle surfaces, the drop spreads rapidly to a local maximum spreading ratio, pauses and retracts only slightly, and then begins to spread again. Drop oscillation occurs until surplus kinetic energy is dissipated, and final equilibrium is reached.

As shown in Figure 3, during initial spreading (first several micro-seconds), the spreading curves are very similar for the five substrates indicating that kinetic energy of the drop is dominating and rolling motion sets in at the contact line[23] during this stage. Directly after impact ($t \leq 5$ μs), $D(t)$ increases with t^n with $n = 0.60 \pm 0.10$, 0.51 ± 0.06, and 0.54 ± 0.06, for impact speeds of 2.21, 4.36, and 12.2 m/s, respectively. These values of n are close to the theoretical value ($n = 0.5$) for spreading dominated by kinetic energy.[24]

As the drop spreads and kinetic energy of the drop is dissipated or converted into the surface energy due to the increase in surface area of the spreading drop, the liquid-substrate interaction becomes more important and the spreading curves for the various substrates are different. With decreasing equilibrium contact angle, the drop spreads further over a longer period of time. The key stages of micron scale drop spreading on substrates will be discussed in detail in the following sections.

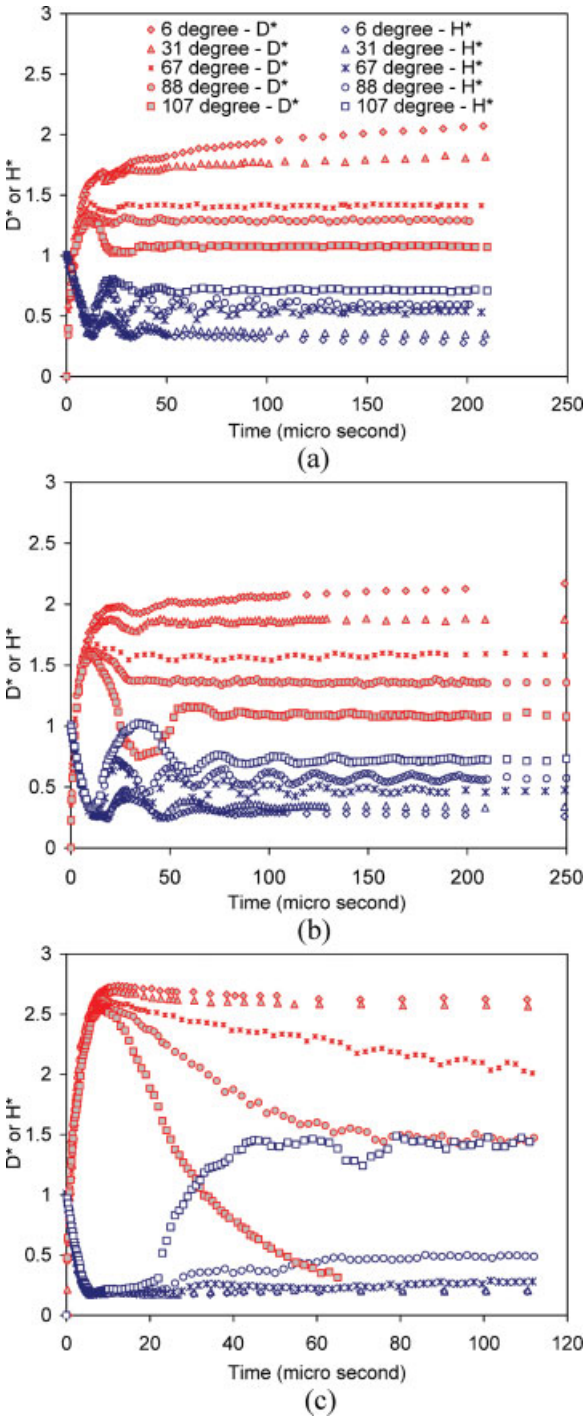

Figure 3. Variation of spreading ratio D^* and dimensionless drop height H^* with time: (a) U_0 = 2.21 m/s, D_0 = 40.9 μm, We = 2.77, Oh = 0.0165; (b) U_0 = 4.36 m/s, D_0 = 48.8 μm, We = 12.8, Oh = 0.0151; (c) U_0 = 12.2 m/s, D_0 = 50.5 μm, We = 103, Oh = 0.0148.

[Color figure can be viewed in the online issue, which is available at www.interscience.wiley.com.]

Maximum spreading ratio, D^*_{max}

The maximum spreading ratio (D^*_{max}) is an important parameter in DOD inkjet printing, because it significantly affects the dot size left by the inkjet drop on a substrate after evaporation.[14] Several equations,[8–13] based on experimental results of millimeter-scale impaction, have been developed to predict D^*_{max}. The only equation completely based on micron scale drops, i.e. application-scale for inkjet printing, was constructed by Asai et al.[14]; however, this equation does not

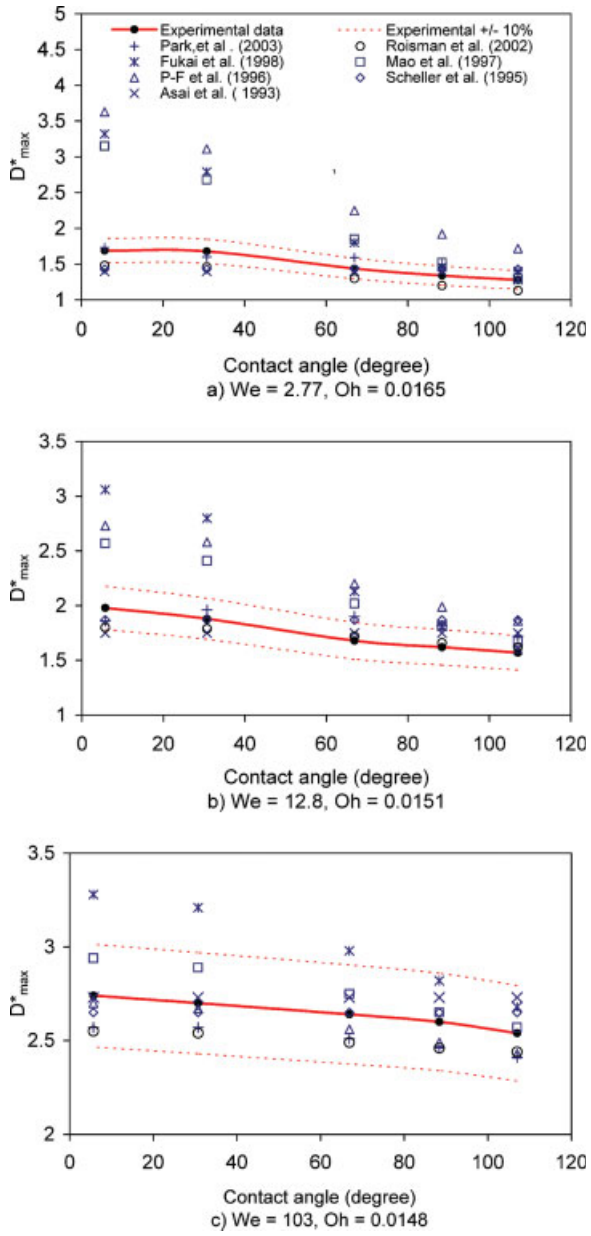

Figure 4. Comparison of experimental results with predictions of seven equations for D^*_{max}.

[Color figure can be viewed in the online issue, which is available at www.interscience.wiley.com.]

include the effect of contact angle. In Figure 4, our experimental results are compared with predictions from these seven equations. Here, the experimental results of D^*_{max} for surfaces with low-contact angle (6 and 31°) are the first peak in the D^* vs. time curves although, after a short pause, the drop continues to spread to larger D^*. The subsequent spreading is driven by the wettability of the surface.

At $We = 103$, all equation predictions agree with the experimental values within 10%, except for the equation of Fukai et al.,[11] which overpredicts D^*_{max} for low-contact-angle surfaces by more than 10%. And, the dependence of D^*_{max} on the equilibrium contact angle is small, varying from 2.54 to 2.74 for contact angle ranging from 107 to 6°. For low-We impaction ($We = 2.77$ and 12.8, see Figures 4a and b, respectively), most of the equations provide acceptable predictions for large contact angle surfaces (88° and 107°). However, for low-contact angle surfaces, the discrepancy between predictions and experimental results are significant, for example, up to 50% for the equation of Mao et al.[10] when $We = 2.77$ and $\theta = 6°$. In contrast, predictions of the equations of Park et al.[13] and Roisman et al.[12] agree with the experimental results with deviation less than 10% for both low- and high-We impactions.

The equation of Park et al. considers not only viscous dissipation, but also energy dissipated during spontaneous spreading, which leads to lower predictions of D^*_{max} for low-contact angle surfaces than those of other models. The spontaneous spreading energy dissipation term accounts for energy dissipated when a drop at zero impact velocity spontaneously spreads to its equilibrium position, and its magnitude increases as the contact angle decreases. It is significant only at very low impact speeds and low-contact angles, as illustrated in Figure 5, where spontaneous spreading dissipation is compared with kinetic energy of an impacting drop, both scaled by total surface energy of the impacting drop, $\pi D_0^2 \gamma$. Dimensionless spontaneous spreading energy dissipation, E_{diss}, is equal to $1 - \left[\frac{1}{4}(2 - 3\cos\theta + \cos^3\theta)\right]^{1/3}$, and dimensionless initial kinetic energy E_k, is equal to $We/12$. At small We and low-contact angle, the magnitudes of these quantities are of the same order of magnitude. Thus, if only viscous dissipation is considered, as in equations of Mao et al.,[10] Pasandideh-Fard et al.,[9] and Fukai et al.,[11] predictions do not agree well with experimental results for small We and low-contact angle.

The predictions of the equations of Roisman et al.[12] agree with the experimental results with deviation less than 10% for both low- and high-We impactions and all five contact

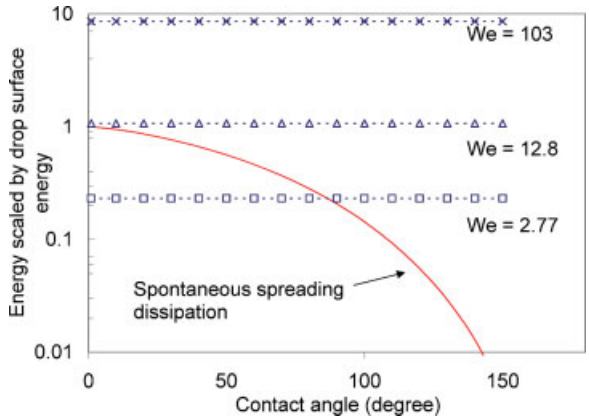

Figure 5. Comparison between spontaneous spreading dissipation and kinetic energy of impacting drop, scaled by total surface energy of impacting drop $\pi D_0^2 \gamma$.

The solid line is the dimensionless spontaneous dissipation, E_{diss}, and the dash line is the dimensionless initial kinetic energy, $E_k = We/12$. [Color figure can be viewed in the online issue, which is available at www.interscience.wiley.com.]

Table 4. Dimensionless Time, t^*_{max}, Oscillation Time and Dissipation Time

Drop Diameter (μm)	Impaction Speed (m/s)	Contact Angle (°)	t_{max} (μs)	t^*_{max}[a]	Spreading/ Retracting Time (μs)	Oscillation Time[b] (μs)	Dissipation Time[c] (μs)
40.9	2.21	6	18	0.97	O(10,000)	10.9	470
		31	17	0.92	O(10,000)		
		67	13	0.70	O(10)		
		88	12	0.65	O(10)		
		107	12	0.65	O(10)		
48.8	4.36	6	24	2.14	O(1,000)	14.2	669
		31	20	1.79	O(1,000)		
		67	12	1.07	O(10)		
		88	11.2	1.00	O(10)		
		107	10	0.89	O(10)		
50.6	12.2	6	12.4	2.99	–	15.0	719
		31	11.6	2.80	–		
		67	9.4	2.27	O(100)		
		88	8	1.93	O(10)		
		107	8	1.93	O(10)		

[a]Scaled by D_0/U_0.
[b]Oscillation time $\sim t_{ca} = (\rho R_0^3/\gamma)^{1/2}$.[6]
[c]Dissipation time $\sim \rho R_0^2/\mu$.[6]

angles. Besides the viscous dissipation based on a viscous creeping flow between two approaching discs, the model of Roisman et al.[12] also uses a dynamic contact angle and includes the work performed by the radial forces applied from the wall to the contact line.

The equation of Asai et al.,[14] which is a correlation of experimental results for micron drop impaction, predicts within 10% of the experimental results even though the model does not consider the effect of surface-liquid interactions. The empirical equation of Scheller et al.[8] also gives a good fit. Their equation is obtained by correlating experimental results against the dimensionless group Re^2Oh, neglecting the effect of the equilibrium contact angle.

Dimensionless time, t^*_{max}

The time to reach D^*_{max} is usually scaled by D_0/U_0 to obtain a dimensionless time t^*_{max}. Chandra and Avedisian[7] assumed that $t^*_{max} = 1$, whereas Pasandideh-Fard et al.[9] used an analytical approach to obtain $t^*_{max} = 8/3$, and Mao et al.[10] and Park et al.[13] adopted this value in their models. Our experimental results for t_{max} and t^*_{max}, listed in Table 4, show a strong dependence on impact speed, as well as equilibrium contact angle, and t^*_{max} increases with increasing We and/or decreasing θ. At the highest impact speed (U_0 = 12.2 m/s), t^*_{max} is about triple that at the lowest impact speed (U_0 = 2.21 m/s). In these experiments, t^*_{max} ranges from 0.65 to 2.99, indicating that it is not acceptable to treat t^*_{max} as a constant.

Beyond initial spreading: Evolution of drop on substrate

(a) Retraction and rebound

After reaching D^*_{max}, retraction of the drops depends on equilibrium contact angle and impaction speed. For very hydrophilic substrates, such as thermally oxidized silicon wafers and glass slides, the retraction of the contact area is insignificant because the liquid layer is arrested at the contact line (see Figures 2 and 3). As θ increases, the tendency to retract increases. Dimensionless height of the retracting drop at maximum retraction, H^*_{max}, vs. We is shown in Figure 6. For hydrophilic surfaces (θ = 6, 31, 67, and 88°), H^*_{max} decreases with increasing We, suggesting that even at higher impact velocity, no rebounding will occur. In contrast, for the hydrophobic surface with θ = 107°, H^*_{max} increases with We, and rebounding occurs when H^* exceeds a critical value. In these experiments for θ = 107°, rebounding occurs for impaction speeds of 10.6 and 12.2 m/s, but not for impaction speeds of 2.21 and 4.36 m/s. The rebounding criterion of Mao et al.,[10] which predicts rebounding when excess rebound energy $E^*_{ERE} > 0$, correctly predicted rebounding in our micron scale drop impaction experiments except in one case where $E^*_{ERE} \sim 0$.

(b) Relaxation to equilibrium

Before an impacting drop reaches its equilibrium state on a substrate, it goes through relaxation (spreading/retracting, oscillation and dissipation of surplus energy). Three forms of relaxation curves (D^* vs. t) observed in these experiments are shown in Figure 7. In the first case (curve a in Figure 7),

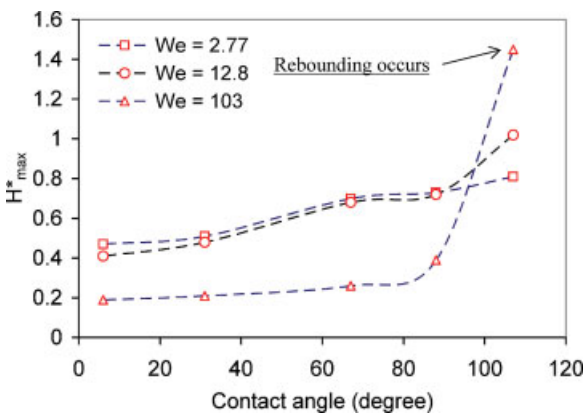

Figure 6. Maximum dimensionless height (H^*_{max}) during drop retraction vs. θ for three Weber numbers.

Note that rebounding only occurs at We = 103 and θ = 107°. [Color figure can be viewed in the online issue, which is available at www.interscience.wiley.com.]

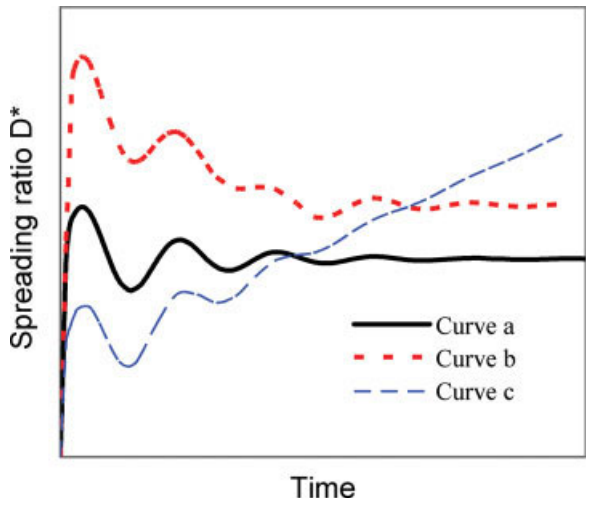

Figure 7. Three types of relaxation curves.

[Color figure can be viewed in the online issue, which is available at www.interscience.wiley.com.]

the contact base of the drop overshoots its equilibrium position during the spreading stage, and then retracts and oscillates around its equilibrium position. This mode can be seen in Figures 3a and b for $\theta = 67$, 88, and 107°. For the second case (curve b in Figure 7), the contact base of the drop significantly overshoots its equilibrium position, and oscillations in D^* and H^* are subsequently observed as the drop retracts toward its equilibrium position, as shown in Figure 3c for $\theta = 67$ and 88°. For the third case (curve c in Figure 7), the contact base of the drop undershoots its equilibrium position, and after a short pause, the drops starts to spread again with oscillations in D^* and H^* again observed for times which are comparable to this initial rapid spreading phase. The drop continues to spread over times much longer than the first inertially-driven spreading under these conditions, as shown in Figures 3a and 3b for $\theta = 6$ and 31°.

The time scale of kinetic (or initial) spreading is D_0/U_0, and in the present experiments ranged from 10 to 20 μs. After a spreading drop reaches D^*_{max}, depending on contact angle, the drop may spread or retract until D^* equals the spreading ratio at the equilibrium drop position, D^*_e, which can be estimated from a relationship given by Ford and Furmidge.[25] The total time from impaction until this occurs is referred to as spreading/retracting time even though some drops on low-contact angle substrates may not retract at all. Continuous spreading mainly due to the interfacial energy takes about 1~10 ms for low contact angle surfaces, while for higher contact angle surfaces the retraction time is $O(10)$~$O(100)$ μs (see Figure 3 and Table 4). Both spreading and retracting times depend on the separation of D^*_{max} from D^*_e. The time scales of the oscillation period and viscous dissipation are $(\rho R_0{}^3/\gamma)^{1/2}$ and $\rho R_0{}^2/\mu$, respectively,[6] where R_0 is the radius of drop before impaction. The values of these parameters (spreading/retracting, oscillation and viscous dissipation time) are compared in Table 4. The dissipation time scale is much larger than the oscillation time scale, and thus, many oscillation cycles may occur before the surplus energy is dissipated. The spreading/retracting time is comparable to the oscillation time for the first case (curve a in Figure 7), but larger than the oscillation times for the other two cases. In the present experiments, the amplitude of oscillation decreases with time and after about 500 μs, oscillation becomes undetectable in all cases. For hydrophilic surfaces (6 and 31°), spreading continues after oscillations are no longer detectable.

Continuous spreading occurs for low θ (6 and 31°), and $We = 2.77$ and 12.8, as shown in Figure 8. Assuming that the relationship between D^* and dimensionless time t^* (scaled by capillary time, $t_{ca} = (\rho R_0^3/\gamma)^{1/2}$) has the form $D^* = gt^{*n}$,[26] where g and n are parameters determined by data fitting using power-law regression. Here, the parameter n depends on the wettability of surfaces, and is in the range of 0.07–0.09 for the glass slide and 0.02–0.03 for the SiO_2 wafer. These values are lower than the exponent of 1/10 of Tanner's law, which is valid for complete wetting. Since the contact angles of glass and SiO_2 are 6 and 31°, respectively, n should decrease with increasing contact angle because the interfacial force decreases as contact angle increases. For a given We, the values of g are almost identical for glass slide and SiO_2 wafer. Note that the values of D^*_{max} for $We = 2.77$ and 12.8 are almost identical in these experimental results (see Figures 4a and b), suggesting that g should be scaled by D^*_{max}.

Comparison between micron- and millimeter-scale drop impaction

In order to identify the effect of drop size on the drop impaction process and to determine the validity of the dimensionless description of the drop impaction process, we conducted millimeter-scale drop impaction tests with the same We and Oh and almost the same cos θ as those for the micron drop impaction tests discussed in the previous

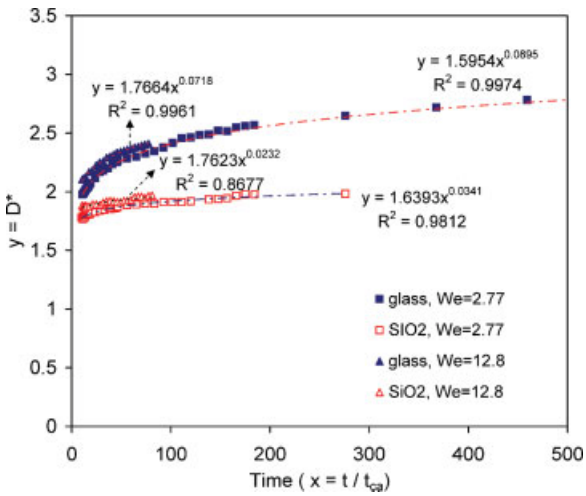

Figure 8. Drop spreading on substrates with low θ: glass slide $\theta = 6°$, and SiO_2 wafer, $\theta = 31°$.

The time is scaled by the capillary time $t_{ca} = (\rho R_0{}^3/\gamma)^{1/2}$, also shown in Table 4. [Color figure can be viewed in the online issue, which is available at www.interscience.wiley.com.]

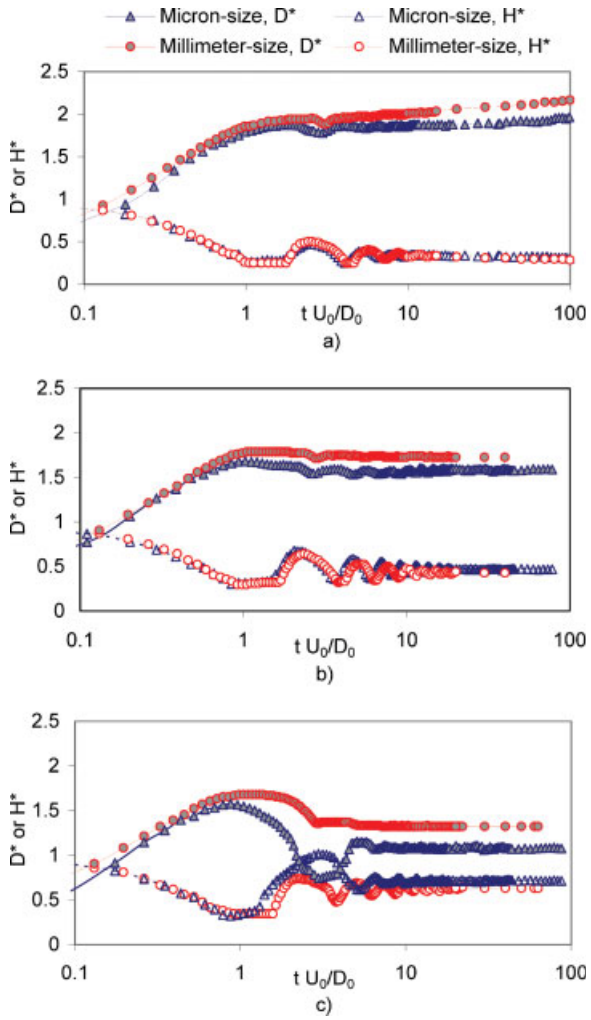

Figure 9. Comparison of dimensionless drop contact diameter and height for millimeter and micron drops impactions with *We* = 12.7–12.8, Oh = 0.0148–0.0151 and surfaces: (a) SiO_2 Wafer, θ = 31 and 24° for micron and millimeter drops, respectively; (b) 9:1 OH/CH_3 SAM on gold coated silicon wafer, θ = 67 and 62° for micron and millimeter drops, respectively; (c) 100% CH_3 SAM on gold coated silicon wafer, θ = 107 and 99° for drop and millimeter drops, respectively.

[Color figure can be viewed in the online issue, which is available at www.interscience.wiley.com.]

sections (see Table 2). The results for the millimeter drops (D_0 = 2.23 mm) are compared with those for the micron drops (D_0 = 48.8 μm) in Figure 9, where the diameter of the contact area is scaled by D_0, and time is scaled by D_0/U_0 (11.2 μs and 3.84 ms for micron-scale drops and millimeter-scale drops, respectively). The mixture of glycerin and water used for the millimeter drop impaction has a slightly lower surface tension than the distilled water used for the micron drop impaction, and the contact angles of the millimeter drop are slightly smaller than those of the micron drops on the same substrate (see Table 3).

As shown in Figures 9, with the same *We* and *Oh*, the millimeter and micron drop impactions on the same substrates exhibit very similar spreading, retraction and oscillation behavior, except that the micron-scale drops show a slightly lower D^* and retract more strongly from D^*_{max}. During initial spreading, the behaviors of millimeter and micron drops are almost identical. When spreading approaches D^*_{max}, the millimeter drops have a higher spreading ratio. The difference in D^*_{max} for millimeter drops, and the corresponding micron drops is less than 20 % for most of the cases. The millimeter and micron drops start to recoil at almost the same dimensionless time, but the millimeter drop recoils less and more slowly than the corresponding micron drop. During relaxation, the oscillation cycles for the two sizes of drops are very close, and the decaying behaviors of the oscillation amplitudes are similar. The final spreading ratio of the millimeter drop is slightly larger than that of the micron drop. These differences also exist for other experimental conditions (*We* = 2.77 and 103).

Two plausible reasons for the differences in the D^* vs. t^* curves for the millimeter and micron drops are: (1) The contact angle of the millimeter drop on a given substrate is lower than that of the micron drop; distilled water and mixtures of glycerin and water were used to generate the micron and millimeter drops, respectively; and (2) The role of gravity in millimeter drop impaction is more significant than in micron drop impaction.

Another millimeter-scale test was conducted where *We* and *Oh* were essentially identical to those for the micron-

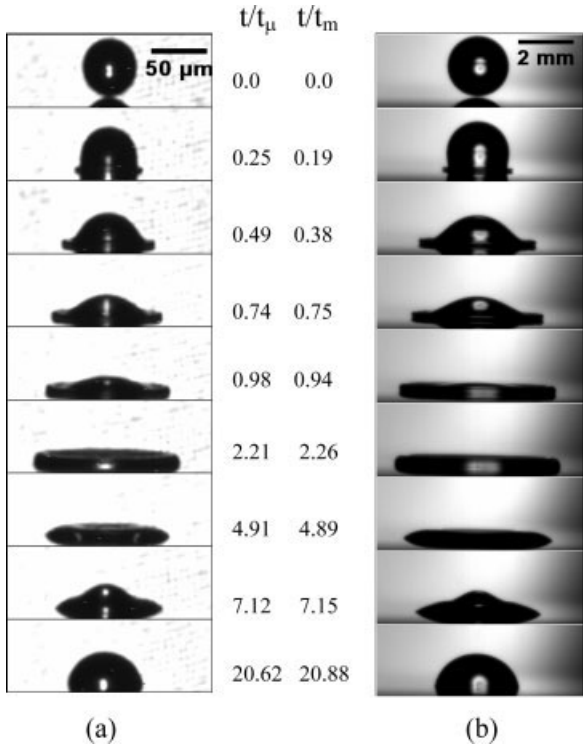

Figure 10. Comparison of (a) 50.5-μm drop, and (b) 2.23-mm drop impaction sequences at *We* = 103–105, *Oh* = 0.0146–0.0148 and θ = 98–99°, t_μ = 4.14 μs and t_m = 1.34 ms.

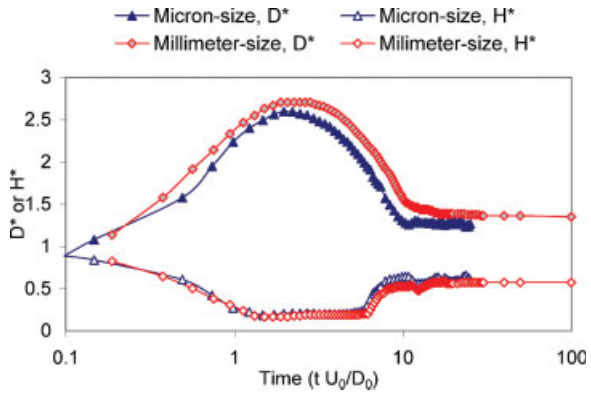

Figure 11. Comparison of millimeter and micron drop impaction curves at *We* = 103–105, *Oh* = 0.0146–0.0148 and θ = 98–99°.

[Color figure can be viewed in the online issue, which is available at www.interscience.wiley.com.]

scale tests (We = 103 - 105, Oh = 0.0146 - 0.0148, and the contact angles for the micron and millimeter drops were adjusted by varying the ratios of OH/CH_3 applied to the silicon wafer until the contact angles were 98 and 99° for the micron and millimeter drops, respectively. For the same We, Oh, and θ, profiles of millimeter and micron drop deformation are almost identical at similar dimensionless time (see Figure 10), the D^* vs. t^* curves are closer and the difference in D^*_{max} is smaller (compare Figures 9 and 11). However, a difference between the micron- and millimeter-scale drop dynamics during the impaction process persists. These observations lead us to conclude that differences in contact angle—an influence which can be eliminated in practice—explains some of the differences in the micron- and millimeter-drop impaction results, but gravitational effects remain a source of discrepancy.

The Froude number $Fr = U_0^2/(R_0 g)$, the ratio of ratio of inertia force to gravitational forces, is useful in quantifying the relative influence of gravity. As shown in Table 5, Fr is much larger for the micron drops than that for the millimeter drops, differing by a factor of several hundred to over one thousand. The role of gravity in millimeter drop impaction is clearly of more significance than in micron drop impaction. For the impaction process of millimeter drops, especially during the spreading stage, the effect of gravity is non-negligible when the impaction speed is low. For example, at an impaction speed of 0.27 m/s, the gravitational force is up to 15% of the inertial force. Therefore, the effect of gravity leads to a larger D^*_{max} for millimeter drops than for micron drops. We can also see that the Bond number, $Bo = \rho g D_0^2/\gamma$, the ratio of gravitational force to surface tension forces, is about 0.82 for millimeter size drops, but only $O(10^{-4})$ for micron drops, suggesting that gravity causes the observed final resting dimensionless contact diameter to be larger for millimeter drops.

In Table 5, the Bond number for the micron drops is shown to be extremely small while the Froude number is extremely large, suggesting that the effect of gravity on micron-drop impaction is insignificant and consequently that the inkjet drop impaction process on substrates is not dependent on printing direction.

Conclusion

Experimental results for smooth flat surfaces indicate that scaling of micron drop impactions from millimeter drop impaction, based on the dimensionless numbers Oh, We and cos θ, is largely valid. This similitude facilitates study of dynamics relevant to DOD techniques by allowing much larger drops and less rapid impact processes at the larger scale to be studied as a surrogate for the actual process. Plots of D^* vs. tU_0/D_0 for micron and millimeter drops at the same dimensionless numbers are similar except that D^* of millimeter drops is usually slightly larger during the whole process. The difference can be mostly attributed to the larger effect of gravity on the millimeter drop impaction dynamics and final state.

Existing equations of D^*_{max} give good predictions with deviations less than 10% from the present experimental results for We = 103, even though most of these equations were constructed based on the millimeter drop impaction experiments. For low-We impaction, the predictions of most of these equations do not agree well with the present experimental results, especially on low-contact angle surfaces. However, the equations of Park et al.[13] and Roisman et al.[12] are exceptions since both provide good predictions (less than 10%) for both high- and low-We impaction.

The dimensionless time to reach D^*_{max} is not a constant as was assumed in several previous investigations, but ranges from 0.6 to 2.99, depending on We and contact angle. Drop retraction from D^*_{max} depends on both We and θ. For hydrophilic surfaces, the retraction height decreases as We increases; by contrast, for hydrophobic surfaces, the retraction height increases with We and rebounding occurs when We exceeds a critical value. The rebounding model of Mao

Table 5. Comparison of Froude (*Fr*) and Bond (*Bo*) Numbers for Millimeter and Micron Drops Under the Same *Re* and *We*

Regime	Impaction Speed (m/s)	Drop Size (μm)	*Re*	*We*	*Fr*	*Bo*
Micron drop	2.21	40.9	100.9	2.77	2.44×10^4	2.28×10^{-4}
	4.36	48.8	238	12.8	7.95×10^4	3.24×10^{-4}
	12.2	50.5	689	103	6.01×10^4	3.47×10^{-4}
Millimeter drop	0.27	2230	101.6	2.74	6.67	0.82
	0.58	2230	241	12.7	30.8	0.82
	1.67	2230	700	105	255	0.82

et al.[10] correctly predicts rebounding in the present experiments for most cases.

Acknowledgments

This work was supported by National Textile Center (C02-GT07) and C05-GT07), and also by NASA Microgravity Fluid Physics Program (NAG3-2739).

Literature Cited

1. Worthington AM. On the forms assumed by drops of liquids falling vertically on a horizontal plate. *Proc R Soc London*. 1877;25:261–272.
2. Worthington AM. A second paper on the forms assumed by drops of liquids falling vertically on a horizontal plate. *Proc R Soc London*. 1877;25:498–503.
3. Rein M. Phenomena of liquid-drop impact on solid and liquid surfaces. *Fluid Dyn Res*. 1993;12:61–93.
4. Yarin AL. Drop impact dynamics: Splashing, spreading, receding, bouncing. *Ann Rev Fluid Mech*. 2006;38:159–192.
5. Crooks R, Cooper-White J, Boger DV. The role of dynamic surface tension and elasticity on the dynamics of drop impact. *Chem Eng Sci*. 2001;56:5575–5592.
6. Schiaffino S, Sonin AA. Molten droplet deposition and solidification at low weber numbers. *Phys Fluids*. 1997;9:3172–3187.
7. Chandra S, Avedisian CT. On the collision of a droplet with a solid-surface. *Proc R Soc London Ser A*. 1991;432:13–41.
8. Scheller BL, Bousfield DW. Newtonian drop impact with a solid-surface. *AIChE J*. 1995;41:1357–1367.
9. Pasandideh-Fard M, Qiao YM, Chandra S, Mostaghimi J. Capillary effects during droplet impact on a solid surface. *Phys Fluids*. 1996;8:650–659.
10. Mao T, Kuhn DCS, Tran H. Spread and rebound of liquid droplets upon impact on flat surfaces. *AIChE J*. 1997;43:2169–2179.
11. Fukai J, Tanaka M, Miyatake O. Maximum spreading of liquid droplets colliding with flat surfaces. *J Chem Eng Jpn*. 1998;31:456–461.
12. Roisman IV, Rioboo R, Tropea C. Normal impact of a liquid drop on a dry surface: Model for spreading and receding. *Proc R Soc London Ser A*. 2002;458:1411–1430.
13. Park H, Carr WW, Zhu JY, Morris JF. Single drop impaction on a solid surface. *AIChE J*. 2003;49:2461–2471.
14. Asai A, Shioya M, Hirasawa S, Okazaki T. Impact of an ink drop on paper. *J Imaging Sci Techn*. 1993;37:205–207.
15. Attinger D, Zhao Z, Poulikakos D. An experimental study of molten microdroplet surface deposition and solidification: Transient behavior and wetting angle dynamics. *J Heat Transfer*. 2000;122:544–556.
16. Kim HY, Park SY, Min K. Imaging the high-speed impact of micro-drop on solid surface. *Rev Sci Instrum*. 2003;74:4930–4937.
17. van Dam DB, Le Clerc C. Experimental study of the impact of an ink-jet printed droplet on a solid substrate. *Phys Fluids*. 2004;16:3403–3414.
18. Dong HM. Drop-on-demand drop formation and deposition. Georgia Institute of Technology; 2006. *Doctoral dissertation*.
19. Dong HM, Carr WW, Morris JF. An experimental study of drop-on-demand drop formation. *Phys Fluids*. 2006;18:072102.
20. Dong HM, Carr WW, Morris JF. Visualization of drop-on-demand inkjet: Drop formation and deposition. *Rev Sci Instrum*. 2006;77:085101.
21. Bain CD, Troughton EB, Tao YT, Evall J, Whitesides GM, Nuzzo RG. Formation of monolayer films by the spontaneous assembly of organic thiols from solution onto gold. *J Am Chem Soc*. 1989;111:321–335.
22. Leopoldes J, Dupuis A, Bucknall DG, Yeomans JM. Jetting micron-scale droplets onto chemically heterogeneous surfaces. *Langmuir*. 2003;19:9818–9822.
23. Reznik SN, Yarin AL. Spreading of an axisymmetric viscous drop due to gravity and capillarity on a dry horizontal wall. *Int J Multiphas Flow*. 2002;28:1437–1457.
24. Biance AL, Clanet C, Quere D. First steps in the spreading of a liquid droplet. *Physical Review E*. 2004;69:016301.
25. Ford RE, Furmidge CGL. Impact and spreading of spray drops on foliar surfaces. *Wetting Soc Chem Industry Monograph*. 1967;25:417–432.
26. Alteraifi AM, Sherif D, Moet A. Interfacial effects in the spreading kinetics of liquid droplets on solid substrates. *J Colloid Interf Sci* 2003;264:221–227.
27. Timmermans J. The physico-chemical constants of binary systems in concentrated solutions. New York: Interscience; 4 v; 1959.

Manuscript received Jan. 5, 2007, revision received Apr. 21, 2007, and final revision received July 17, 2007.